ELSEVIER

Applied Surface Science 197–198 (2002) 688–698

applied surface science

www.elsevier.com/locate/apsusc

Encoding of holographic grating and periodic nano-structure by femtosecond laser pulse

Masahiro Hirano[a,*], Ken-ichi Kawamura[a], Hideo Hosono[a,b]

[a]*Hosono Transparent Electro-Active Materials (TEAM) Project, ERATO, Japan Science and Technology, Kawasaki 213-0012, Japan*

[b]*Materials and Structures Laboratory, Tokyo Institute of Technology, Nagatsuda 226-8503, Japan*

Abstract

By fully utilizing distinct features of femtosecond (FS) pulses such as ultra-short time domain and good coherence, we have successfully encoded micro-gratings and multi-dimensional periodic nano-structures either on or beneath surfaces of versatile materials including dielectrics, semiconductors, metals and plastics. In the setup for the encoding, a regenerative amplified pulse from a mode locked Ti:sapphire laser was split into two beams, then overlapped on the top surface or in the interior of the materials to give a ~50 μm spot. The optical paths of the two beams should be adjusted precisely within ~30 μm to induce the interference. Use of the third harmonic generation (THG) from air made the adjustment possible not restricted from colliding angles. Surface relief type gratings due to laser ablation and refractive index type gratings resulted from structural changes in silica glasses, embedded gratings in diamond, gratings capable of light coupling and decoupling to a $LiNbO_3$ wave guide, and two-dimensional nano-structures in silica glass are demonstrated as examples. We expect the present technique to open up a frontier of diffractive optics with the formation of periodic nano-structures applicable to emerging devices such as planar wave guides, quantum dots and photonic crystals.

Keywords: Femtosecond laser; Holographic grating; Micro-machining; Nano-structure; Silica glass; $LiNbO_3$; Diamond

1. Introduction

Femtosecond (FS) pulses from a mode locked Ti: sapphire laser are characterized by an ultra-short time domain with good coherence over the whole pulse duration. These features allow for unique applications when applied to material processing as schematically illustrated in Fig. 1. First, FS laser pulses are extremely short, leading to very high peak powers due mostly to the temporal compression of the laser energy.

Such high peak powers can process almost all kinds of materials, which need not be very photosensitive, typically by laser ablation [1–3]. This energy can also induce structural changes, inevitably accompanied by refractive index modulation [4,5].

Second, with the aid of non-linear effects such as multi-photon absorption and self-focusing, we can concentrate the laser energy onto a very small spot, smaller than the diffraction limit. Nano-scale structures may be formed in this way. In addition, the pulse terminates before the completion of energy transfer from photo-excited electrons to the lattice, which minimizes thermal effects during the machining process and makes the process cleaner [1,2,6,7], specifically

* Corresponding author.
E-mail address: m-hirano@ksp.or.jp (M. Hirano).

0169-4332/02/$ – see front matter
PII: S0169-4332(02)00446-4

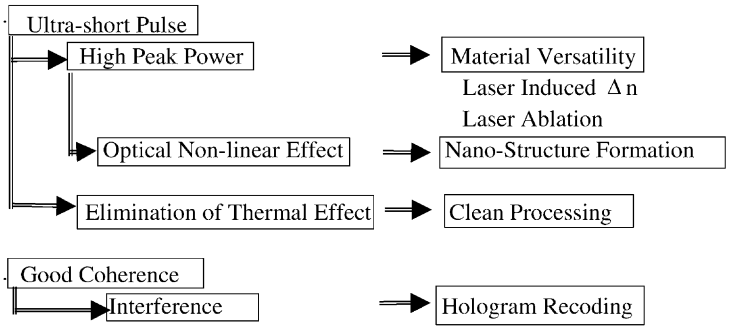

Fig. 1. Features of FS laser pulses as applied to material processing.

when only a single pulse is involved. Good coherence [8], which is another distinct feature of the FS pulse, makes it possible to encode holograms in various materials by splitting a single pulse into multiple beams and allowing them to interference. Comprehensive use of these features may provide a unique opportunity for encoding periodic nano-structures in versatile materials. With this goal in mind, we have recently developed a "hologram encoding system by interfering FS laser pulse" and have succeeded in encoding a variety of periodic structures in various materials, including transparent dielectrics, semiconductors, plastics and metals [9–11]. The minimum structure size is reduced to the nano-meter scale [12].

In this paper, we will describe mechanism and experimental procedure for encoding holograms by FS pulses. In addition, we will show typical examples of encoded holograms or periodic structures, which include both surface relief and embedded micro-gratings fabricated by a two beam laser exposure technique, and two-dimensional structures composed of periodically aligned dots and trapezoids, which were encoded by a double exposure technique.

2. Mechanism for hologram encoding by femtosecond pulses and experimental setup

2.1. Encoding mechanism

As FS laser pulses exhibit good coherency over the entire pulse duration, interference takes place when two FS pulse beams split from a single pulse overlap with each other both spatially and temporally. The interference pattern resulting from this overlapping can be transferred to materials to encode micro-gratings when the laser energy in enhanced region of the interference pattern exceeds the threshold for laser ablation or structural changes of the material. Exploiting non-linear effects may allow for the fabrication of nano-scale structures.

Hologram encoding system by FS laser pulses is quite similar to conventional two beam laser exposure techniques, except that FS laser pulses are used instead of a continuous wave light from a gas laser having a long coherent length. To ensure spatial and temporal overlap, an optical delay line and a mechanism for detecting time coincidence of the two beams with a spatial accuracy of ∼micrometer is required. It is also desirable for the time coincidence measurement to be independent of the angle between the interference beams. By varying this angle, we can control over fringe intervals in gratings and over shapes of unit elements in two-dimensional periodic structures.

2.2. Experimental setup

Fig. 2 shows a schematic diagram of an experimental setup for grating encoding using FS laser pulses. As a light source, we used a Ti:sapphire laser system consisting of a Ti:sapphire oscillator, a stretcher, a regenerative amplifier pumped by the second harmonic of an Nd:YAG laser and a compressor. It generated 800 nm light pulses with a repetition rate of 10 Hz, pulse duration of ∼100 FS (an effective coherence length of ∼30 μm), and a maximum energy of 3 mJ per pulse. A FS laser pulse from the laser system was divided into two beams by a half-silvered mirror. The separated beams propagated along different optical paths with

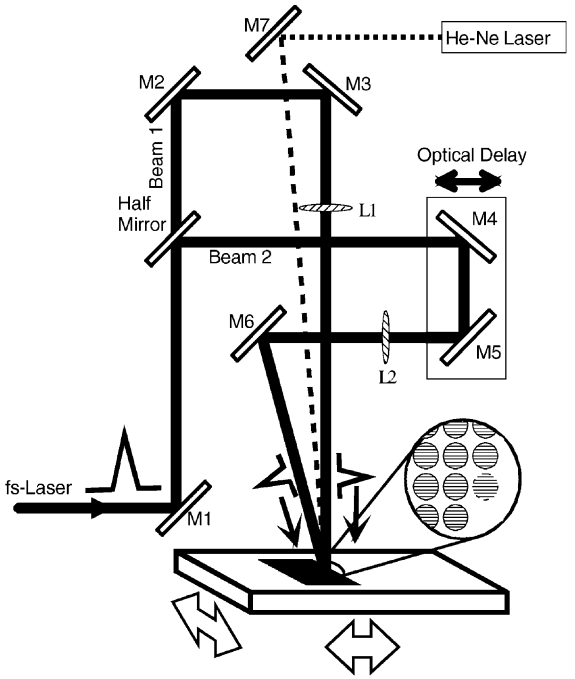

Fig. 2. Experimental setup for hologram encoding system using FS laser pulses.

one having a variable path length (optical delay line). The pulse energy was varied from 10 to 3,000 μJ. The two beams were focused onto a single spot 50–100 μm in diameter by lenses with a focal length of 5 cm. The angle of intersection (θ) between these two beams was varied from 10 to 160°. The spatial length of each optical path was equalized with a precise movement of mirrors in the optical delay line, while monitoring the time coincidence signal. THG from air was used for the signal [13], as described later.

Once the time coincidence of the two beams was realized, samples were placed at the beam focus position. Encoding of the gratings was confirmed in situ by detecting diffracted light from an incident He–Ne laser. Fig. 3 shows that both spatial and temporal coincidences were simultaneously required for encoding gratings.

2.3. New adjustment technique with third harmonic generation in air

It has been reported that THG is induced when an intense FS laser pulse is focused in various gases such as air [14] or argon [15], and the mechanism has been discussed theoretically [16]. We have applied this phenomenon to monitor the time coincidence of the two FS pulses.

When pulse energy of the first FS laser beam exceeds more than 1.5 mJ per pulse, a blue spot is observed at the beam center of the far field pattern,

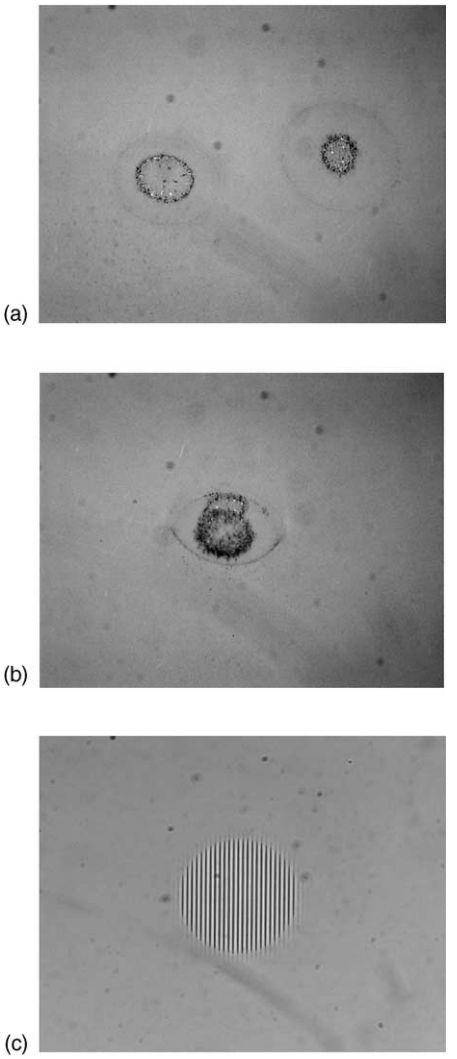

Fig. 3. Images showing that spatial and temporal coincidence of two FS laser beams is required for encoding gratings. (a) No gratings are recorded when two FS beams are not in spatial coincidence. (b) No gratings are recoded when two FS beams are in coincidence spatially, but not temporally. (c) Gratings are encoded when two FS beams are in coincidence both spatially and temporally.

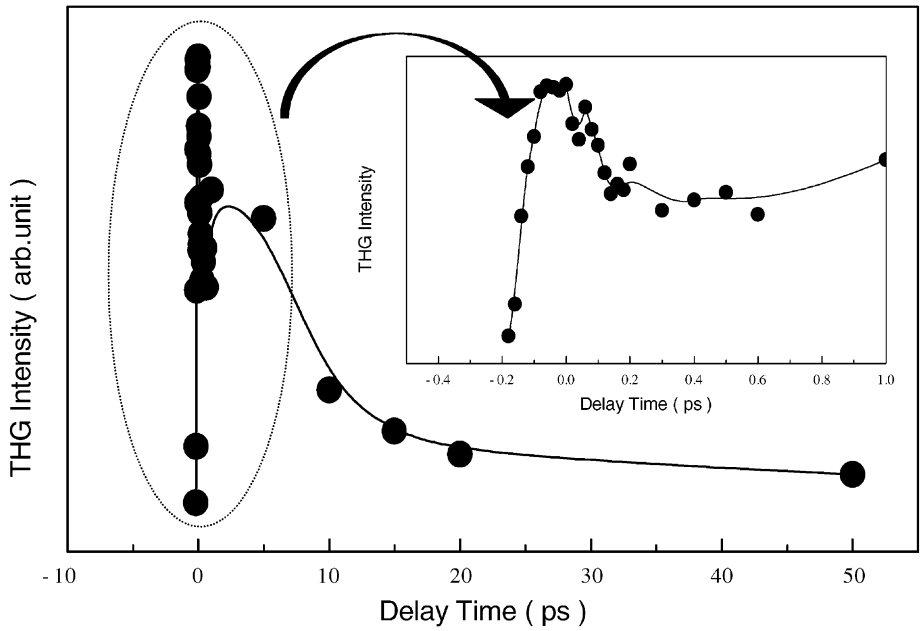

Fig. 4. THG light intensity as a function of delay time between two FS laser pulses. Inset: expanded curve around zero delay time.

which was confirmed as the third harmonics of the laser fundamental (800 nm) at 266 nm. The THG was not observed when the pulse was focused in vacuum, indicating that air was responsible for THG. Then, a second focused beam, having an energy of 50 μJ per pulse, which was too small to induce the THG light by itself, was directed at the focal point so as to overlap spatially with the first beam. The far field pattern of the second beam on the luminescence screen yielded only weak white continuum light without the blue spot, likely due to the self phase modulation in air when the relative time delay of the two pulses was large. While tuning the optical path length, the blue THG spot suddenly appeared at the center of the white continuum spot. Fig. 4 shows the THG intensity in the second beam as a function of the delay time calculated from the change in the optical path length.

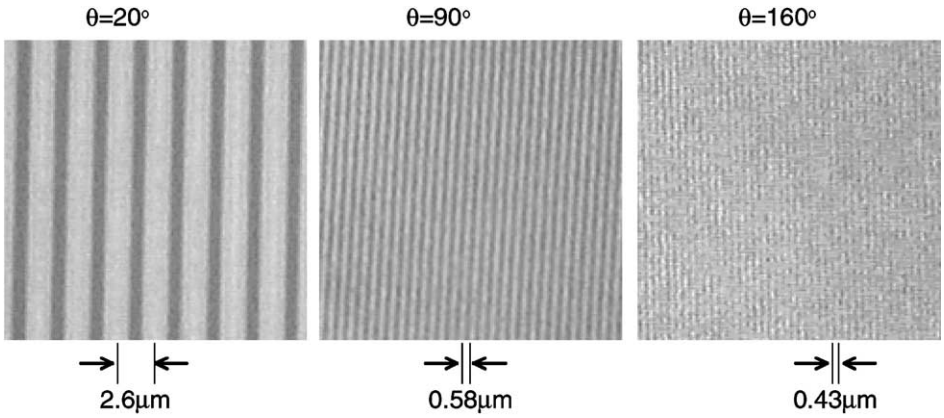

Fig. 5. Optical microscope images of gratings recorded in silica glasses for various beam intersecting angles (θ). Fringe interval d varies with θ according to the equation $d = \lambda/[2\sin(\theta/2)]$.

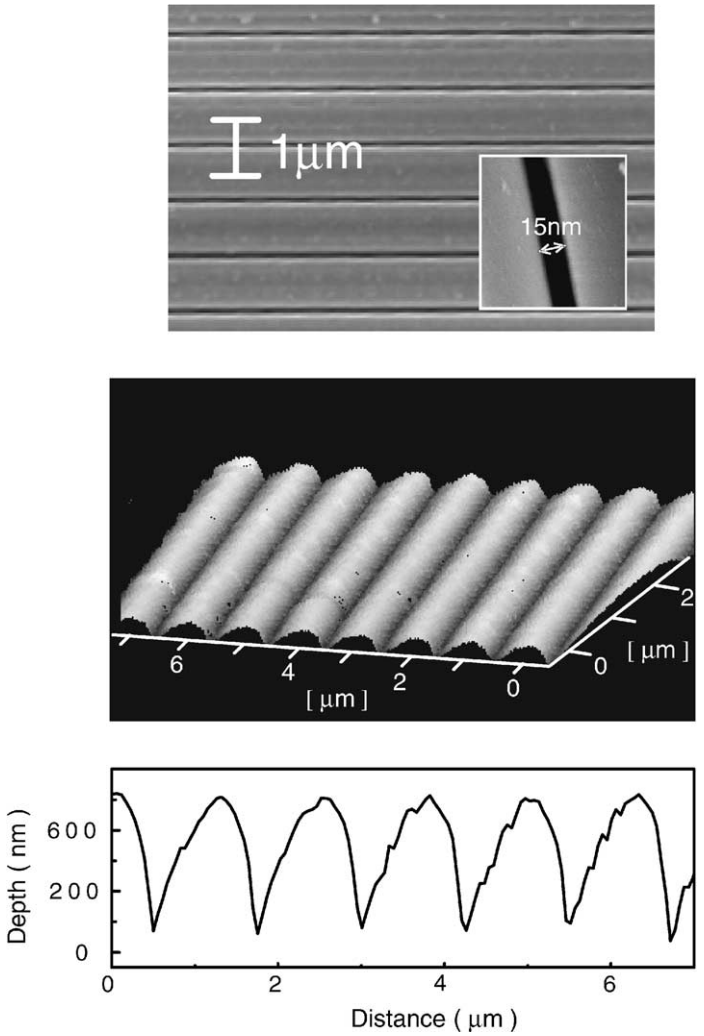

Fig. 6. SEM image (upper) and AFM profile (lower) of a grating encoded in silica glass.

The intensity increases abruptly as the delay time approaches zero from below. The rise time for the THG enhancement estimated from the inset figure was ∼200 FS, which is in reasonable agreement with a pulse width of ∼100 FS. With a further increase in the delay time, the intensity decreases sharply at first. The decrease then becomes gradual and is still observed at delay times above 50 ps. Despite the gradual decay on the long delay time side, the peak in Fig. 4 is sharp enough to determine the exact time coincidence of the two FS pulses. The trend in Fig. 4 was basically independent of the angle of intersection of the two beams, as expected from the inherent nature of THG in the gas phase. The use of THG in air makes it possible to arrange for the time coincidence of two FS pulses over a wide range of angles of intersection.

3. Examples of encoded holograms

3.1. Surface relief type holograms

3.1.1. Bulk silica glass

When the intersecting beams were focused onto the surface, surface relief type gratings were encoded due to material ablation. Fig. 5 shows surface relief gratings

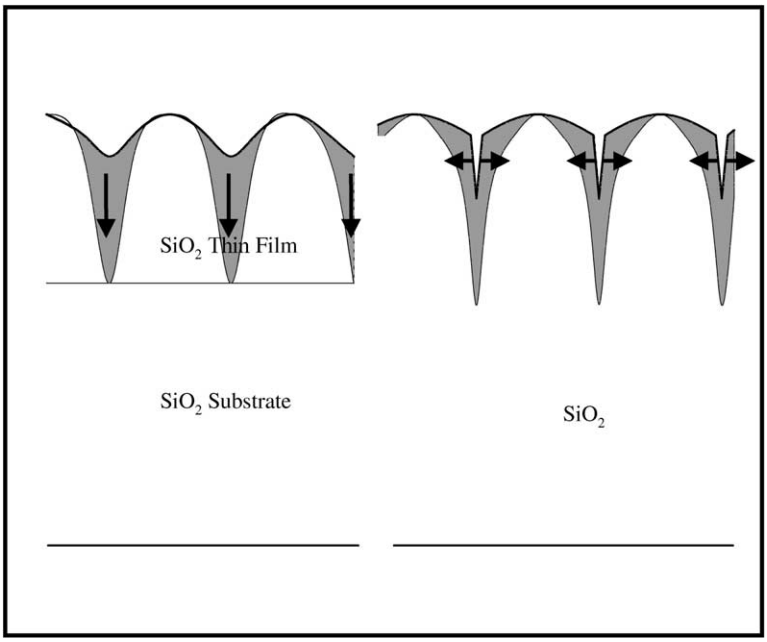

Fig. 7. Schematic representation of local compaction induced by interfering FS laser pulses on silica glass. In case of bulk silica glass, compaction generates tensile forces directed parallel to the surface, yielding periodic narrow valley structures (right). In case of silica thin films, the tensile force is directed perpendicular to the surface, and produces a shallow, periodic surface modulation (left).

encoded in silica glass for several θ values with a total fluence of 0.3 mJ per pulse. Each grating forms a circle with a diameter of ~100 μm and is composed of parallel fringes with a constant spacing equal to $\lambda/[2\sin(\theta/2)]$, where λ is the laser wavelength (800 nm). This observation gives a clear evidence that the gratings were encoded as the results of interference between the two FS pulses of the fundamental wavelength (800 nm). The formation of a periodic valley structure at the surface is revealed by AFM images. The deposition of debris or molten materials on the surface indicates that the grating structure results from laser ablation at this fluence level.

Infrared spectra suggested O–Si–O bond angles in the laser-irradiated area suffered photo-induced changes, leading to the densification of the silica glass. Such structural changes have been observed in silica glasses during high energy ions implantation or neutron bombardment; densification typically saturates at ~3% [17]. As this compaction is accompanied by a refraction index increase of ~0.7%, a refraction index modulation type grating can be simultaneously formed beneath the surface relief type grating.

High resolution images of the grating acquired with a field emission scanning electron microscope (SEM) (Fig. 6) show periodic valleys in the internal structure of the grating. These valleys are very narrow, down to 15 nm. The compaction of silica glass in very localized areas due to intense laser irradiation generates tensile forces directed parallel to the surface as schematically shown in Fig. 7, which likely to play an important role in the formation of the periodic valleys.

3.1.2. Silica glass thin film

Surface relief type gratings with a valley depth as shallow as 3.5 nm were recorded in thin film silica on a silicon wafer by reducing the total fluence to 0.015 mJ. The surface profile of the fabricated grating was smooth and neither small deposits nor macroscopic laser damage or cracking were observed at this fluence, suggesting that the formed grating resulted from the densification of the films (Fig. 7), not from laser ablation. The valley depth of the grating (3.5 nm) relative to the film thickness (114 nm) supported this suggestion, as it coincides with the saturation level (~3%) of radiation-induced densification in amorphous SiO_2. A

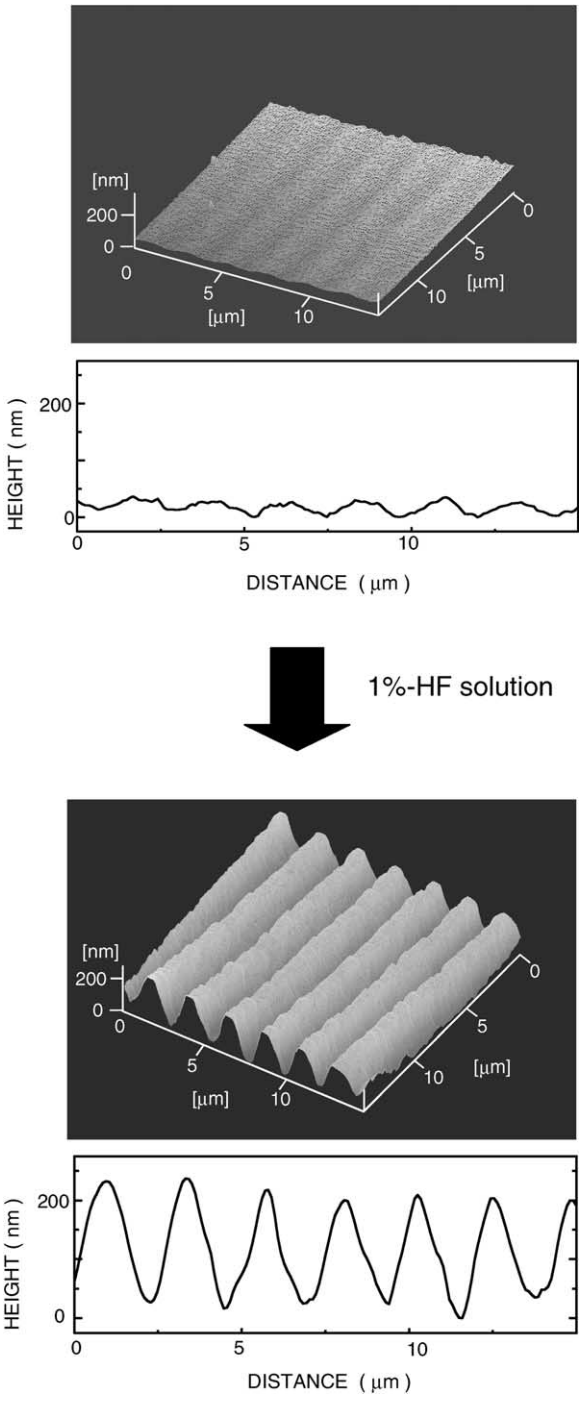

Fig. 8. AFM images of surface relief type gratings encoded in silica thin films before and after etching by 1% HF solution. The valley depth was deepened due to preferential etching in the densified areas.

difference in the properties of undensified and densified amorphous SiO_2 is manifested in the etching rates during stress enhanced corrosion [18]. We utilized this phenomenon to deepen the valley of the gratings. An AFM image and a cross-section of grating structures formed by etching with 1% HF solution (Fig. 8) shows that etching increases the depth of the valley by a factor of 5–6 relative to that before etching. In other words, chemical etching has converted the refractive index modulation type grating into a surface relief type grating.

3.2. Embedded type grating

When the focal point of the interfering FS laser pulses was positioned inside the target materials, an embedded grating is recorded through a refractive index modulation, either due to structural alternations such as densification in silica glass, crystallographic phase changes from crystalline to amorphous states, or the formation of micro-pores due to the evaporation of a small amount of the materials.

Such an embedded grating was recorded inside a diamond crystal as demonstrated in Fig. 9. Confocal microscopic images reveal the grating lies 0.45–1.05 μm beneath the surface. Raman spectra for the grating encoded area suggest that the refractive index modulation was caused by a structural change from diamond to diamond-like carbon or amorphous carbon [19].

3.3. Optical coupling and decoupling elements in optical wave guide

The diameters of the recorded gratings (∼50 μm) are similar to the width and depth of optical wave guides (∼10 μm). Thus, these gratings are capable of coupling and decoupling of light to wave guides. We encoded two gratings on a wave guide fabricated on $LiNbO_3$ substrate. Fig. 10 demonstrates that He–Ne laser light can be coupled and decoupled to the wave guide through these gratings.

4. Formation of two-dimensional periodic nano-structure

Two-dimensional periodic structures can be formed by a double exposure technique. A series of optical

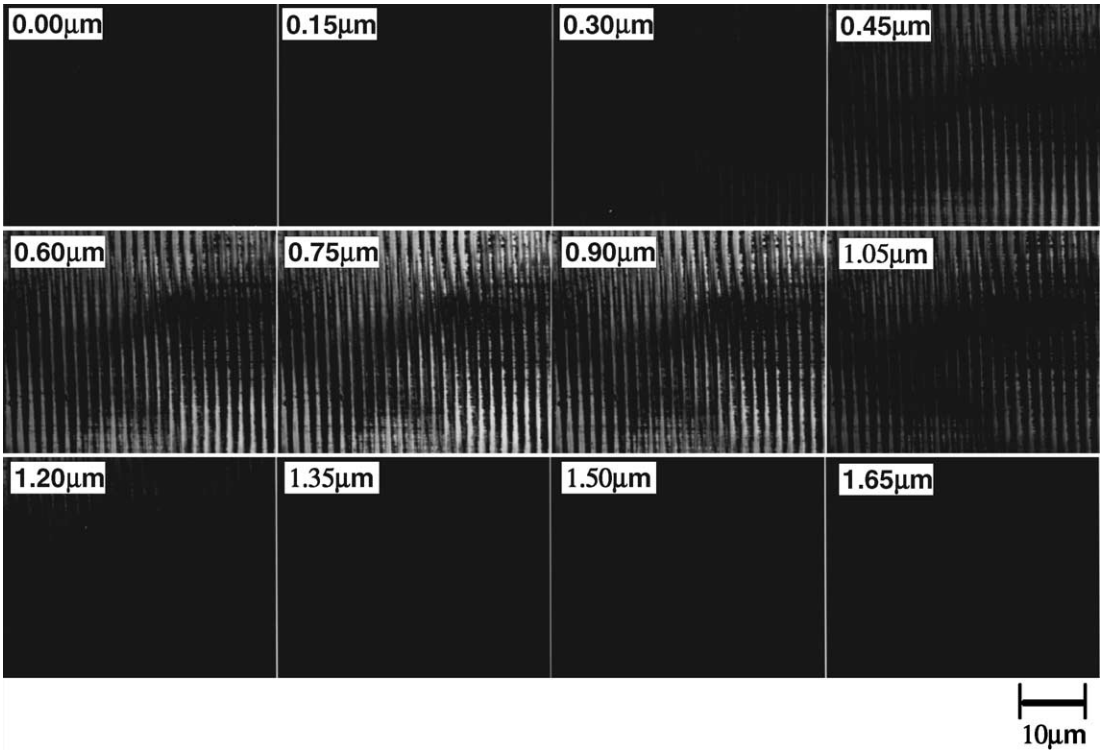

Fig. 9. A series of confocal microscope images of an embedded grating encoded in diamond. The grating is located 0.45–1.05 μm beneath the surface.

microscope images of the gratings in Fig. 11 demonstrate the double exposure procedure. Photos (a) and (b) in this figure show gratings with diameters of ∼15 and ∼50 μm encoded by laser pulse energies of 40 and 100 μJ, respectively. After the first grating was encoding, the samples were rotated by 90° and a second grating was recorded superposed on the first grating. The resultant structure is not always a simple superposition of two kinds of gratings, but a complicated structure results from interactions between the two encoding processes. Fig. 12 is an SEM image of a crossed grating encoded when energy in the second pulse (80 mJ) was larger than in the first one (40 mJ) with a 45° angle between the beams for both exposures. The periodic vertical lines represent fringes of the grating encoded by the first exposure, since the periodicity of 1.0 μm equals $\lambda/[2\sin(\theta/2)]$. It is noted that an array of round dots with a diameter of ∼140 nm are observed in the center part of the crossed grating. The dots become ellipsoidal as one moves toward the edge of the grating and finely connect with each other to form periodic horizontal lines. Since the first grating was not encoded in the outer area and the spacing is consistent with the second exposure, the horizontal lines here are fringes of the second grating. The formation of the dot array in the central part results from the interaction between the first grating and the incident beams in the second exposure.

When the first pulse energy (80 μJ per pulse) is larger than that of the second pulse (40 μJ per pulse), the resultant structure is composed of periodic narrow valleys recorded by the first exposure and a two-dimensional dot array with exfoliations and cracks around the dots (Fig. 13). The dot array results from the interaction between the periodic valleys and the incident beams in the second exposure. By increasing θ from 45 to 90°, an array of trapezoid structures could be produced; this array looks a simple superposition of two orthogonal gratings (Fig. 14).

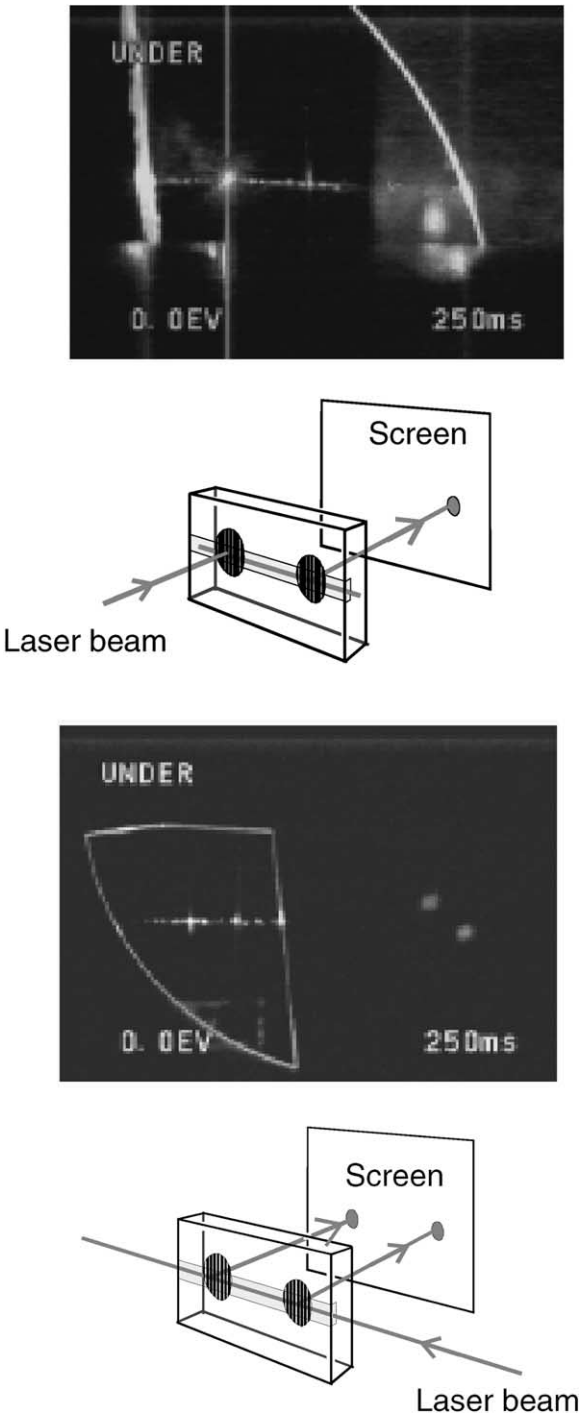

Fig. 10. Photographs of two gratings encoded on an optical wave guide fabricated in $LiNbO_3$. Light coupling and decoupling functions of the gratings are demonstrated.

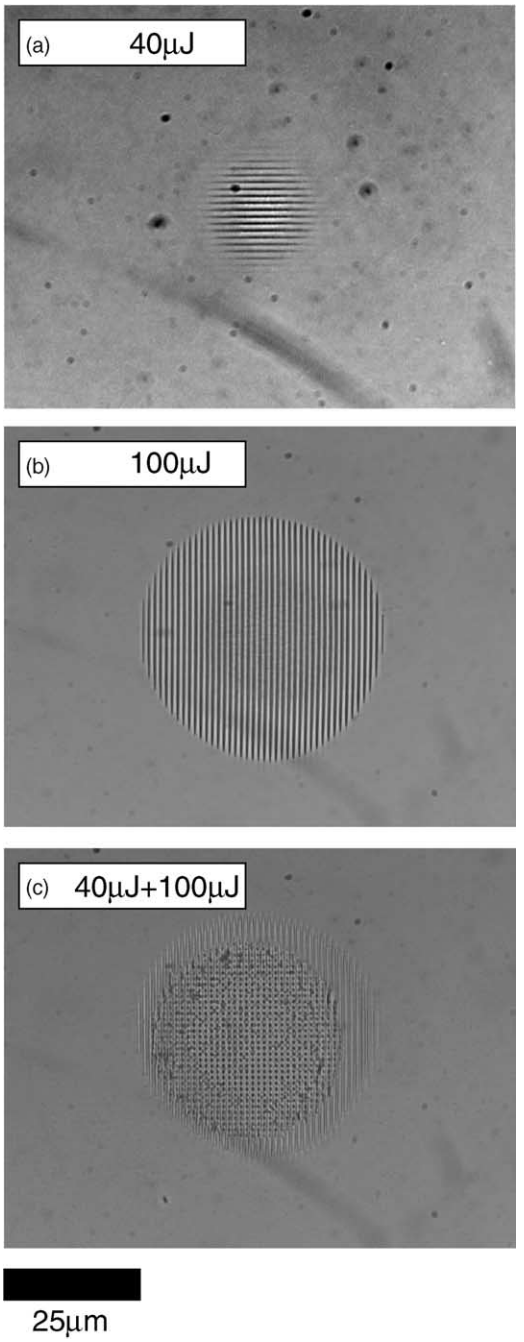

Fig. 11. Procedure for double exposure. (a) Optical microscopic image of a grating encoded at a total laser fluence of 40 μJ per pulse (first grating). (b) Optical microscopic image of a grating encoded at a total laser fluence of 80 μJ per pulse after the sample was rotated by 90° (second grating). (c) Optical microscopic image of a crossed grating, encoded by superposing the second grating onto the first grating.

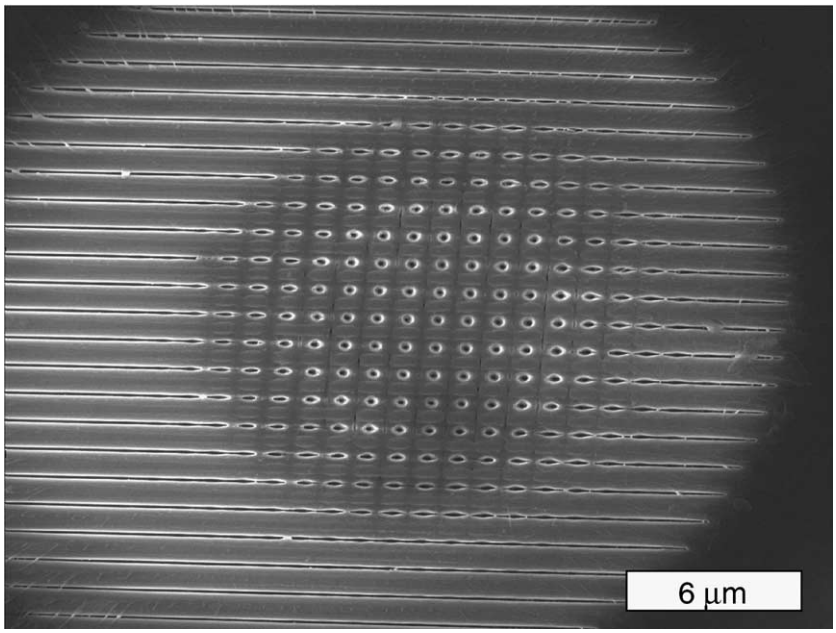

Fig. 12. SEM image of a crossed grating encoded at a total fluence of 40 μJ per pulse for the first exposure and 80 μJ per pulse for the second exposure. The beams intersected at an angle of 45° for both exposures.

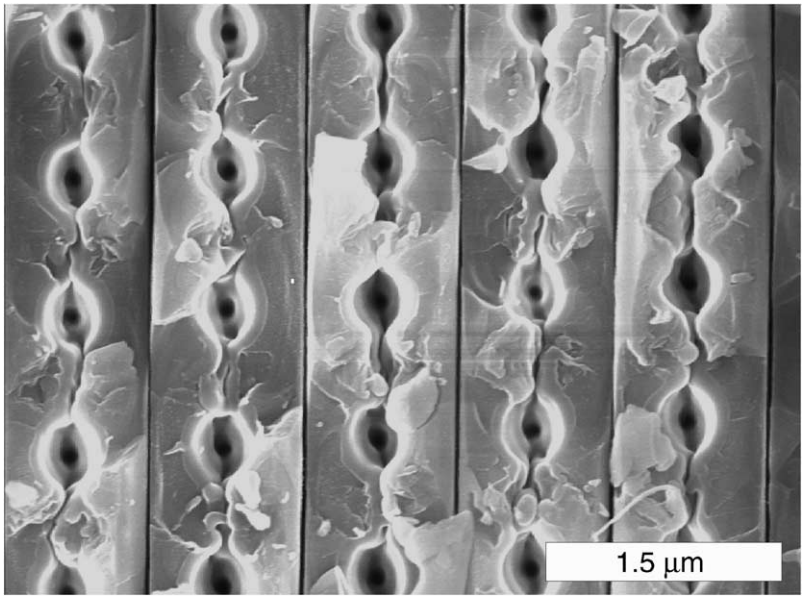

Fig. 13. SEM image of a crossed grating encoded at a total fluence of 80 μJ per pulse for the first exposure and 40 μJ per pulse for the second exposure. The beams intersected at an angle of 45° for both exposures.

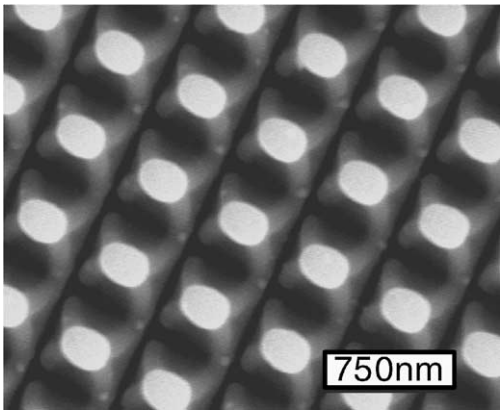

Fig. 14. SEM image of a crossed grating encoded at a total fluence of 100 μJ per pulse and the beams intersected at right angle for each exposure.

These results indicate that the double exposure technique using FS laser pulses offers a new tool for the formation of two-dimensional nano-structures in various kinds of materials.

5. Summary

We have developed a hologram encoding technique using FS laser pulses from a mode locked Ti:sapphire laser. The resulting periodic structures exhibit distinct features summarized as follows:

1. Because of the extremely high energy density, periodic structures can be encoded in almost all kinds of materials including dielectrics, semiconductors, metals and plastics.
2. The periodic structures are formed in small sizes, ∼50 μm in diameter, which is compatible with micro-optic devices such as optical wave guides.
3. The encoding can be performed by a single pulse exposure for micro-gratings or a double exposure for two-dimensional periodic arrays; both minimize thermal effects during processing.
4. Both surface relief and embedded type periodic structures are encoded.
5. Nano-structures with a minimum size down to ∼10 nm could be fabricated with the aid of nonlinear laser–material interactions.

References

[1] E.E.B Campbell, D. Ashkenasi, A. Rosenfeld, Mater. Sci. Forum. 301 (1999) 123.
[2] J. Krüger, W. Kautek, Appl. Surf. Sci. 96–98 (1996) 430–438.
[3] J. Ihlemann, B. Wolff, R Simon, Appl. Phys. A 54 (1992) 363.
[4] J.H. Strickler, W.W. Webb, Opt. Lett. 16 (1991) 1780.
[5] E.N. Glezer, E. Mazur, Appl. Phys. Lett. 71 (1997) 882.
[6] D. von der Linde, K. Sokolowski-Tinten, J. Bialkowski, Appl. Surf. Sci. 109–111 (1997) 1–10.
[7] B.C. Stuart, M.D. Feit, A.M. Rubenchik, B.W. Shore, M.D. Perry, Phys. Rev. Lett. 74 (1995) 2248.
[8] E.P. Ippen, C.V. Shank, Ultra-Short Light Pulses, in: S.L. Shapiro (Ed.), Springer, New York, 1997 (Chapter 3).
[9] K. Kawamura, N. Sarukura, M. Hirano, H. Hosono, Appl. Phys. B 71 (2000) 119.
[10] K. Kawamura, N. Sarukura, M. Hirano, H. Hosono, Jpn. J. Appl. Phys. 39 (2000) L767.
[11] K. Kawamura, N. Sarukura, M. Hirano, H. Hosono, Appl. Phys. Lett. 78 (2000) 1038.
[12] K. Kawamura, N. Sarukura, M. Hirano, H. Hosono, Appl. Phys. Lett. 79 (2001) 1228.
[13] K. Kawamura, N. Ito, N. Sarukura, M. Hirano, H. Hosono, Rev. Sci. Instrum. 73 (2002) 1711.
[14] S. Backus, J. Peatross, Z. Zeek, A. Rundquist, G. Taft, M.M. Murnane, H.C. Kapteyn, Opt. Lett. 21 (1996) 665.
[15] C.W. Siders, N.C. Thrner III, M.C. Downer, A. Babine, A. Stepanov, A.M. Sergeev, J. Opt. Soc. Am. B 12 (1996) 330.
[16] G. Marcus, A. Zigler, Z. Henis, J. Opt. Soc. Am. B 16 (1999) 792.
[17] S.K. Sharma, D.W. Matson, J.A. Philpotts, T.L. Roush, J. Non Cryst. Solids 68 (1984) 99.
[18] F.N. Schwettman, D.J. Dexter, D.F. Cole, J. Electrochem. Soc. 120 (1973) 1566.
[19] J. Roberson, Adv. Phys. 35 (1986) 317.